Ocean Engineering 363 (2026) 126436

Contents lists available at ScienceDirect

Ocean Engineering

journal homepage: www.elsevier.com/locate/oceaneng

Research paper

The influence of mass optimization on the energy absorption efficiency of a submerged body of a two-body wave energy converter

Mahdi Nazari Berenjkoob [a,b], J.F.M. Gadelho [a], Hassan Ghassemi [b,c], C. Guedes Soares [a,*]

[a] Centre for Marine Technology and Ocean Engineering (CENTEC), Instituto Superior Técnico, Universidade de Lisboa, Portugal
[b] Department of Maritime Engineering, Amirkabir University of Technology, Tehran, Iran
[c] School of Ocean Engineering, Harbin Institute of Technology, Weihai, China

ARTICLE INFO

Keywords:
Submerged body
Total mass
Optimum mass
Critical mass
Two-body wave energy converter

ABSTRACT

A procedure is proposed to minimise the submerged body's total mass in a two-body wave energy converter. To this end, three modelling steps are considered, with two default values: the absorber buoy geometry and the wave characteristics. The total mass, which includes both the submerged body's mass and its hydrodynamic added mass, is calculated based on the absorber buoy's specifications and its wave-energy absorption bandwidth. In the first step, the submerged body's optimal mass is achieved 66% of the buoy's mass. The second step is the effect of the body's shape on the model's efficiency. With an optimal mass and proper shape for the submerged body, the maximum power is absorbed, about 62% more than the single-body power, in the resonance region. Moreover, the modelling method establishes identical conditions for comparing the performance of multiple bodies during energy absorption. It was found that two important criteria for the body's shape, which are the ratio of its hydrodynamic coefficients to the wave period, significantly affect the model's efficiency. The results show that higher efficiencies are achieved when a geometrically suitable body substantially reduces the added mass and radiation damping of the model's buoy relative to its free oscillation.

1. Introduction

Wave energy is a promising renewable source due to its high-power potential and availability, both onshore and offshore (Ramos-Marin and Guedes Soares, 2025). Generally, in Wave Energy Converter (WEC) devices, wave power is captured via the interactions between two bodies. One body is always on the water surface, where it interacts with incoming waves, while the other one is either submerged (in the two-body WECs) or fixed on the seabed (in the single-body WECs). PowerBuoy and Seabased WECs are examples of two-body and single-body WECs, respectively (Gaspar et al., 2025; Chen and Zhang, 2025). The relative motion of the WEC's bodies generates electrical power via the combination of a generator with a Power Take-Off (PTO) system, which is generally hydraulic or direct-drive (Zakaria, 2025; Chen and Zhang, 2025).

Most WEC devices require optimisation to progress to the commercial phase. This optimisation can involve their buoy, submerged body, or PTO specifications (Gaspar et al., 2025; Berenjkoob et al., 2021). The buoy's reaction to the incident waves is more important than the other reactions. Hence, the first step is to design the buoy, followed by the WEC's submerged body, PTO system, and, finally, the mooring system.

Multiple procedures have been developed to enhance the efficiency of WECs by optimizing the geometry of both the buoy (Berenjkoob et al., 2021; Garcia-Teruel and Forehand, 2019) and submerged body (Martin et al., 2017; Beatty et al., 2019). Additionally, mechanisms have been introduced to improve the PTO system (Gaspar et al., 2024; Li et al., 2020; Chen and Zhang, 2025) as well as the mooring systems (Berenjkoob et al., 2019b; Xu et al., 2019a). These studies have taken practical steps to enhance the efficiency of two-body WECs. Some of them are described in the rest of the paper and utilised. As the primary focus is on the geometric design of the WEC's submerged body, the mooring system and mechanisms to improve the PTO system are not discussed here and can be considered for future design steps.

The first step in the WEC's design is the geometric design of the absorber buoy to maximise energy absorption from the dominant waves at a predetermined offshore site. In practice, other parts of the WEC, such as the PTO system and the WEC's submerged body, are designed to improve the buoy's hydrodynamic performance. The geometry of the buoy was addressed by Ahmed et al. (2022), Pastor and Liu (2014), and Wang et al. (2025). They compared the absorption performance of

* Corresponding author.
E-mail address: c.guedes.soares@centec.tecnico.ulisboa.pt (C. Guedes Soares).

https://doi.org/10.1016/j.oceaneng.2026.126436
Received 26 December 2025; Received in revised form 4 May 2026; Accepted 4 June 2026
Available online 18 June 2026

several absorber buoys with various geometries to find the best appropriate shape in a single-body WEC. Berenjkoob et al. (2021) presented a design parameter to determine a suitable buoy geometry from among several geometries. The parameter is a ratio of the hydrodynamic coefficients of the buoy, enabling the comparison of different buoys' performance and the selection of the best one. They compared the energy-absorption performance of ten buoys in both irregular and regular waves under identical situations. In this study, as illustrated in Fig. 1, their best-performing buoy is considered the reference buoy for our WEC model.

In terms of the design of the submerged body's geometry, attention is directed towards particular studies by Beatty et al. (2019), Martin et al. (2017), and Liang and Zuo (2017). The importance of a heave plate in the submerged body's design was investigated by Beatty et al. (2019). They analysed the effects of a cylinder, with and without a circular heave plate, on the energy-absorption performance in a two-body WEC. Their findings showed that the WEC's submerged body equipped with a circular heave plate can generate 41% more power than the cylindrical submerged body, based on tests conducted near Vancouver Island. Accordingly, it is essential to incorporate the heave plate into the geometric design of the submerged body, as seen in the Powerbuoy WEC (Beatty et al., 2019).

Martin et al. (2017) and also Liang and Zuo (2017) investigated various submerged body geometries to optimise the body shape of a two-body WEC device. They discovered that the maximum power captured for any geometry occurs at its optimum mass. Moreover, the submerged body's mass can significantly affect the absorber buoy performance of the WEC. Therefore, calculating the optimum mass for the WEC's body (the submerged body) should be a key consideration in designing its geometry, with a focus on the performance range of the WEC buoy. However, there is no established methodology for developing such devices based on their optimal total mass.

To fill this gap, this paper proposes a design method for selecting an appropriate geometry for the WEC's submerged body based upon the features of a pre-specified buoy and its wave energy absorption bandwidth. In practical terms, the wave characteristics determine the absorption bandwidth range to design the WEC's buoy. Subsequently, the buoy and wave characteristics determine the submerged body specifications, including its ideal total mass and the optimal PTO system, in a simultaneous process. Afterwards, some submerged bodies with different geometries are designed to have identical total mass. The total mass is calculated by adding the mass of each submerged body and its hydrodynamic added mass. This design procedure is novel and distinctly different from the aforementioned studies.

The purpose of this study is thus to design the submerged body geometry of a two-body WEC to improve the efficiency of its absorber buoy for maximising energy absorption from the incoming waves. In this context, the buoy geometry, its hydrodynamic features, and the characteristics of the waves must be considered the main inputs in the design of both the submerged body and the PTO system.

2. Methodology

This paper explores different factors, including the design method of the submerged body and how its mass and geometric variations impact the energy-absorption performance of a two-body WEC system. Notably, this study is a follow-up of a previous one (Berenjkoob et al., 2021). It extends prior research on the design of a single-body WEC system into a two-body system. There are two benefits to joining a submerged body under the WEC's buoy and converting a single-body converter system into a two-body WEC system. Firstly, this configuration enables the WEC device to effectively connect with various mooring systems, facilitating deployment in deeper waters. Secondly, the body's dynamics can affect the buoy's hydrodynamics, and improving the WEC's buoy can enhance overall system performance. The importance of a two-body system over a single one has been discussed in relation to other concepts of wave power capture (Rezanejad and Guedes Soares, 2018).

2.1. Two-body WEC model

The PTO system of two-body WECs comprises a rotary generator and a hydraulic circuit, generally modelled as a linear or nonlinear spring-damper system (Zakaria, 2025). Fig. 1 shows three modelling steps for designing the model's body. Step 0 illustrates a schematic view of the heaving WEC model, where its absorber buoy is linked to a submerged body using a combination of a spring and a damper, enabling the absorption of wave energy via their interaction. In this floating model, both the incident wave characteristics and the buoy's geometry remain constant. However, alternative geometries for the submerged body and any specifications for the PTO system can be considered.

In Step 1, the submerged body is simplified to a mass without geometry to calculate its total mass, ensuring the model's buoy falls within the best operating condition. Step 2 shows all effective parameters on the model dynamics in the wave. In other words, a suitable total mass for the submerged body is first calculated based on the specifications of the model's buoy and the wave conditions, as well as using the motion equations of the two-body WEC system, the optimal mode equations of the PTO system, and the derivatives of the absorbed power equation. Then, various shapes are designed for the submerged body, all with the same total mass. Finally, the effect of geometric alterations to the body and the sensitivities of its hydrodynamic parameters on the model's efficiency are studied. This procedure is different from the aforementioned studies.

In this model, the impacts of tidal and marine currents, the PTO's internal friction, and any nonlinear effects are neglected and the mooring system is not considered. It is crucial to emphasise that the final design of any concept must assess its survivability in harsh sea conditions. This evaluation can only be achieved by accounting for nonlinear effects. Various procedures for calculating these nonlinear effects are available, including those proposed by López et al. (2017) and Giorgi and Ringwood (2017).

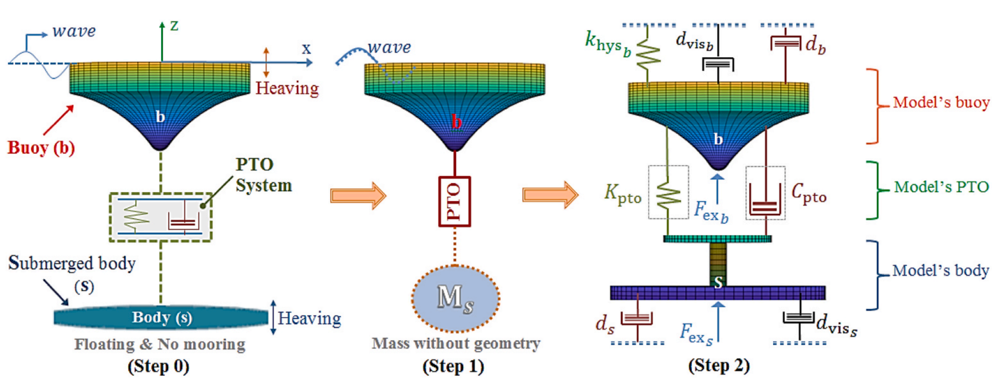

Fig. 1. Scheme diagram of floating the two-body WEC model, free only in heave motion.

Considering regular one-directional waves and the geometric symmetry of the model's buoy and body, the analysis will be limited to heave, surge, and pitch motions. As expected, heave motion has a more significant role in the energy extraction process than surge and pitch motions (Garcia-Teruel and Forehand, 2019). Furthermore, Falnes and Kurniawan (2020) demonstrated the possibility of achieving optimal output power in a heaving two-body WEC system, oscillating in the Z direction, under regular wave excitation. Korde (2003) and Liang and Zuo (2017) also reported that the interaction between the WEC's body and the buoy performs better in heave motion. In this study, heave motion is the effective motion in the energy absorption process, as also addressed in other studies (Falnes and Kurniawan, 2020; Beatty et al., 2019).

2.2. Equations of motion

According to the schematic plan in Fig. 1 and the reasons mentioned, the WEC model oscillates solely in the Z direction, the hydrodynamic forces act only in heave and consist of standard linear decomposition, and the incident waves are harmonic. Following these assumptions, the linear equations of motion for both the model's buoy and submerged body in a coupled system are denoted as follows:

$$(m_b + A_b)\ddot{z}_b + A_{bs}\ddot{z}_s + (d_b + d_{\text{vis}b})\dot{z}_b + d_{bs}\dot{z}_s + k_{\text{hys}}z_b = F_{\text{ex}_b} + F_{\text{pto}}(\text{Buoy}-_{\text{b}}) \tag{1}$$

$$(m_s + A_s)\ddot{z}_s + A_{sb}\ddot{z}_b + (d_s + d_{\text{vis}s})\dot{z}_s + d_{sb}\dot{z}_b = F_{\text{ex}_s} - F_{\text{pto}}(\text{Submerged body}-_{\text{s}}) \tag{2}$$

In these equations, parameters m, A, and d represent the mass, hydrodynamic added mass, and radiation damping coefficient for the model's buoy and submerged body with subscripts b and s, respectively. The two equations align with the motion equations established by Hallak et al. (2024), Rahimi et al. (2024), and Liang and Zuo (2017).

The parameter k_{hys} in Eq. (1) represents the hydrostatic restoring coefficient for the model's buoy. The viscous damping terms of the model's buoy and submerged body are denoted by d_{vis_b} and d_{vis_s}, respectively. The Keulegan–Carpenter number of the model's buoy is very low. So, the inertia force will dominate, making its effect much greater than that of the viscous forces (Berenjkoob et al., 2021).

Furthermore, the effect of viscous damping on the buoy's dynamic behaviour is less significant than that of radiation damping, as indicated by the experimental findings of Beatty et al. (2019) and the numerical results of Liang and Zuo (2017). The buoy's viscous damping is therefore disregarded. However, Liang and Zuo (2017) proposed an equation based on the absorber buoy characteristics that can be used to evaluate the submerged body's viscous damping. This equation is applied only in Step 1, as follows:

$$\zeta_s = \frac{d_{\text{vis}_s}}{2m_b\omega_{n_b}}, \omega_{n_b} = \left(\frac{k_{\text{hys}}}{m_b + A_b}\right)^{0.5} \rightarrow d_{\text{vis}_s} = 2\zeta_s m_b \left(\frac{k_{\text{hys}}}{m_b + A_b}\right)^{0.5} \xrightarrow[\zeta_s = 0.1, 0.125, 0.15]{\substack{\text{Only in} \\ \text{Step 1}}} \tag{3}$$

where ζ_s represents a dimensionless coefficient of viscous damping associated with the submerged body, while ω_{nb} signifies the buoy's natural frequency. The values suggested by Liang and Zuo (2017) for the dimensionless parameter ζ_s are 0.1, 0.125, and 0.150. In Eqs. (1) and (2), the hydrodynamic coupling coefficients arise from the interaction results between the model's buoy and submerged body, and are denoted by parameters d_{bs}, d_{sb}, A_{bs}, and A_{sb}. The hydrodynamic coefficients depend on both the wave properties and the geometry of the buoy and submerged body. Hence, in a specific wave and pre-specified buoy, any variations in the coupling coefficients are solely related to the geometric changes of the body. The wave excitation force on the axisymmetric objects (e.g., the model's buoy and submerged body) as given by (Falnes and Kurniawan, 2020):

$$F_{\text{ex}_j} = a_\omega\left(2\rho g^3 d_j \omega^{-3}\right)^{0.5} \quad j = \text{b}, \text{s}\ (\text{Buoy}-_{\text{b}} : j = \text{b}, \text{Submerged body}-_{\text{s}} : j = \text{s}\ ) \tag{4}$$

The incident wave frequency and its amplitude, the gravitational acceleration, and water density are defined by $\omega = 0.6 - 1.6$ rad/s, $a_\omega = 1$m, $g = 9.806$ m/s^2, and $\rho = 1025$ kg/m^3, respectively. The PTO force, F_{pto}, is obtained as follows (Liang and Zuo, 2017):

$$F_{\text{pto}} = -c_{\text{pto}}\ (\dot{Z}_b - \dot{Z}_s) - k_{\text{pto}}(Z_b - Z_s) \tag{5}$$

In each wave, the velocity and displacement of the model's buoy and submerged body in the heave direction are parameters $\dot{Z}$ and Z, respectively. Parameters k_{pto} and c_{pto} also represent the PTO's specifications, such as its stiffness and damping coefficients, respectively.

The equation of motion in its matrix form is denoted by $[X][Z] = [F]$, where matrix F is the complex amplitude for the wave excitation force, and matrix Z is the complex amplitude for the displacement of the model's buoy and submerged body. Therefore, the matrix X is adapted as an impedance matrix, as defined by Rahimi et al. (2024), Berenjkoob et al. (2019a), and Hallak et al. (2024), as follows:

$$X = \begin{bmatrix} -\omega^2(m_b + A_b) + i\omega(d_b + c_{\text{pto}}) + k_{\text{hys}} + k_{\text{pto}} & -\omega^2 A_{bs} + i\omega(d_{bs} - c_{\text{pto}}) - k_{\text{pto}} \\ -\omega^2 A_{sb} + i\omega(d_{sb} - c_{\text{pto}}) - k_{\text{pto}} & -\omega^2(m_s + A_s) + i\omega(d_s + d_{\text{vis}_s} + c_{\text{pto}}) + k_{\text{pto}} \end{bmatrix} \tag{6}$$

Consequently, the complex amplitude of displacement for the model's buoy and submerged body will be equal to $[Z] = [X]^{-1}[F]$ or $\begin{bmatrix} Z_b \\ Z_s \end{bmatrix} = {}^1/det(X) \begin{bmatrix} X_{22} & -X_{12} \\ -X_{21} & X_{11} \end{bmatrix} \begin{bmatrix} F_b \\ F_s \end{bmatrix}$, which can be further clarified as follows:

$$\begin{cases} Z_b = \dfrac{X_{22}F_b - X_{12}F_s}{X_{11}X_{22} - X_{12}X_{21}} \rightarrow Z_b = \dfrac{\aleph + i\Im + (i\omega c_{\text{pto}} + k_{\text{pto}})\mathscr{R}}{\Gamma + \text{i}\Psi + c_{\text{pto}}(\text{iT} - \Upsilon) + k_{\text{pto}}(T + i\varUpsilon)\omega^{-1}} \\ Z_s = \dfrac{X_{11}F_s - X_{21}F_b}{X_{11}X_{22} - X_{12}X_{21}} \rightarrow Z_s = \dfrac{\wp + i\mathfrak{A} + (i\omega c_{\text{pto}} + k_{\text{pto}})\mathscr{R}}{\Gamma + \text{i}\Psi + c_{\text{pto}}(\text{iT} - \Upsilon) + k_{\text{pto}}(T + i\varUpsilon)\omega^{-1}} \end{cases} \tag{7}$$

where,

$$\begin{cases} \aleph = \omega^2 A_{bs}F_s - \omega^2(m_s+A_s)F_b, F_b = A_\omega\left[2\rho g^3 d_b\omega^{-3}\right]^{0.5} \\ \Im = \omega(d_s+d_{\mathrm{vis}_s})F_b - \omega d_{bs}F_s, \mathscr{R} = F_b+F_s \quad ,F_s = A_\omega\left[2\rho g^3 d_s\omega^{-3}\right]^{0.5} \\ \Gamma = \omega^4\{(m_b+A_b)(m_s+A_s) - A_{bs}A_{sb}\} + \omega^2\{d_{bs}d_{sb} - d_b d_s - k_{\mathrm{hys}}(m_s+A_s) - d_b d_{\mathrm{vis}_s}\} \\ \Psi = \omega(d_s+d_{\mathrm{vis}_s})k_{\mathrm{hys}} - \omega^3\{(m_b+A_b)(d_s+d_{\mathrm{vis}_s}) + (m_s+A_s)d_b - d_{bs}A_{sb} - A_{bs}d_{sb}\} \\ T = -\omega^3(m_b+A_b+m_s+A_s+A_{bs}+A_{sb}) + \omega k_{\mathrm{hys}}, k_{hys} = \rho g\pi r_b^2 \\ \Upsilon = \omega^2(d_b+d_s+d_{\mathrm{vis}_s}+d_{bs}+d_{sb}) \\ \wp = \omega^2 A_{sb}F_b + \{-\omega^2(m_b+A_b)+k_{\mathrm{hys}}\}F_s, \mathfrak{A} = \omega d_b F_s - \omega d_{sb}F_b \end{cases} \tag{8}$$

The above parameters are shown in Eqs. (7) and (8) highlight the particular importance of the hydrodynamic coefficients (A_b,A_s,d_b,d_s,A_{bs}, A_{sb},d_{bs},d_{sb}) in calculating the oscillation amplitudes of the model's buoy and submerged body under the excitation force of the wave with varying frequencies.

$$\begin{cases} c_{\mathrm{pto\ OPTMAL}} = \sqrt{\dfrac{(\Psi^2+\Gamma^2)+\omega^{-2}(T^2+\Upsilon^2)\left(k_{\mathrm{pto\,OPTMAL}}\right)^2 - \omega^{-1}(\Upsilon\Gamma+T\Psi)k_{\mathrm{pto\,OPTMAL}}}{+}} \\ k_{\mathrm{pto\,OPTMAL}} = \omega\dfrac{\Upsilon\Gamma+T\Psi}{T^2+\Upsilon^2} \quad \left.\begin{matrix} k_{\mathrm{pto\,OPTMAL}} \\ c_{\mathrm{pto\ OPTMAL}} \end{matrix}\right\} \rightarrow c_{\mathrm{pto\ OPTMAL}} = \sqrt{\dfrac{\Psi^2+\Gamma^2}{T^2+\Upsilon^2}} \end{cases} \tag{11}$$

2.3. Linear PTO system

The linear PTO system is modelled as a parallel arrangement of a spring and a damper, as shown in Fig. 1. In each wave with a frequency of ω, the power absorbed by the PTO is denoted as $P_{\mathrm{abs}} = 0.5\ c_{\mathrm{pto}}\ \omega^2\ |Z_b - Z_s|^2$ (Berenjkoob et al., 2019a; Rahimi et al., 2024). Then, by substituting Eq. (7) into this expression, an alternative form of the absorption power equation will be expressed as follows:

$$P_{abs} = 0.5c_{\mathrm{pto}}\ \omega^2\left|\frac{\Pi + i\Theta}{\Gamma + i\Psi + c_{\mathrm{pto}}(iT-\Upsilon) + k_{\mathrm{pto}}(T+i\Upsilon)\omega^{-1}}\right|^2, i=\sqrt{-1} \tag{9}$$

where,

$$\begin{cases} \Pi = \aleph - \wp = \{\omega^2(M_b+A_{bs}) - k_{\mathrm{hys}}\}F_s - \omega^2(M_s+A_{sb})F_b \quad M_s = m_s + A_s \\ \Theta = \Im - \mathfrak{A} = \omega(d_s+d_{sb}+d_{\mathrm{vis}_s})F_b - \omega(d_b+d_{bs})F_s \quad M_b = m_b + A_b \end{cases} \tag{10}$$

Note that to avoid the system instability, the stiffness of the PTO spring must always be positive ($k_{\mathrm{pto}} > 0$). For the PTO optimum design, by deriving Eq. (9) partially with respect to k_{pto} and then c_{pto}, the optimal damping and stiffness corresponding to the PTO system will be as follows:

Equation (11) presents the PTO's optimal coefficients, which are approximately similar to the results of Liang and Zuo (2017).

2.4. Model's absorber buoy

The absorber buoy of the WEC model is typically designed with a focus on its absorption bandwidth and performance under wave-resonance conditions. The absorption bandwidth refers to the frequency range of dominant waves at a specific marine location, where the absorbed energy exceeds half of its maximum value (Dai et al., 2025; Gaspar et al., 2025).

In this study, a buoy with appropriate geometry was selected to absorb the maximum wave energy within its absorption bandwidth, drawing on the recent investigation by Berenjkoob et al. (2021). The frequency of the waves in the absorption bandwidth ranged between 0.6 and 1.6 rad/s, with an amplitude of 1m. Fig. 1 illustrates the shape of the buoy, while Fig. 2 shows its hydrodynamic coefficients. The buoy's

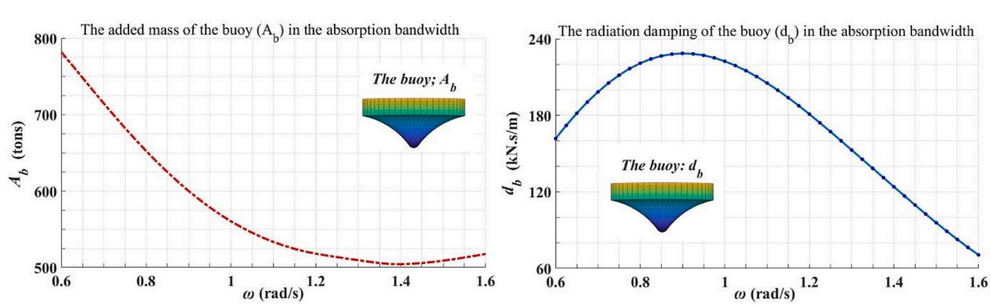

Fig. 2. Hydrodynamic added mass and damping of the model's buoy (Berenjkoob et al., 2021).

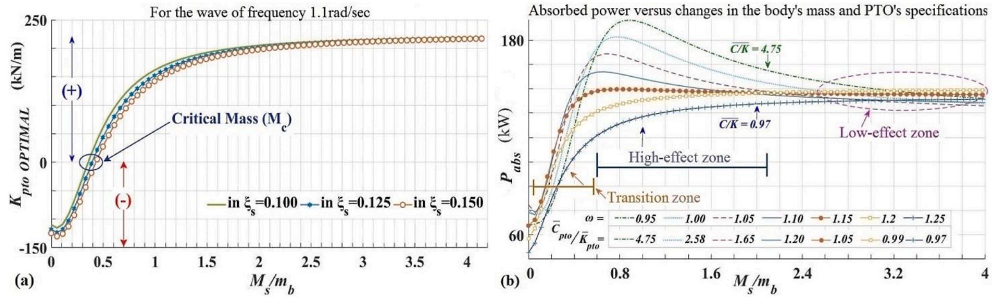

Fig. 3. (a) Influence of the body's mass on the optimal stiffness of the PTO's spring, introducing critical mass of the body in the wave of frequency $\omega = 1.10$ rad/ s $= \omega_{n_b}$ and $\zeta_s = 0.1, 0.125, 0.15$, (b) Impact of the body's mass and the PTO's optimal coefficients on the absorbed power, introducing the high and low-effect and transition zones of the PTO's specifications.

heave natural frequency, radius, and submergence volume are denoted as $\omega_{nb} = 1.1$ rad/s, $r_b = 7.5$ m, and $\forall_b = 883.57$ m^3, respectively.

One can also use another buoy and design a suitable submerged body for it, provided that its hydrodynamic information is available for the given waves. In practice, there are two essential prerequisites for creating the submerged body: the wave characteristics at a specified marine site, and a buoy designed to absorb the maximum energy from these waves.

2.5. Model's submerged body and its optimal mass

This section focuses on a submerged body to enhance the model's buoy performance under specific wave excitation using a defined algorithm. Two main defaults are considered in the design algorithm as follows:

✓ The geometry of the absorber buoy of the WEC model is predetermined.
✓ The specifications of waves within the buoy's absorption bandwidth are given.

The main prerequisites in this algorithm are also outlined as follows:

- The geometry of the submerged body is undefined but symmetrical (in Step 1).
- The model's body is submerged and suspended in the water. The term "model's body" refers to both the submerged body and the body, as depicted in Fig. 1.
- The PTO system must always remain stable (namely, $K_{pto} > 0$) to avoid the singularity.
- The total mass of the body ($M_s = m_s + A_s$) must fall between the critical and the optimum mass values of the body ($M_c < M_s \le M_o$). The term "the body" refers to the model's body (submerged body).

The optimum mass of the submerged body, M_o is described as the maximum mass required for the submerged body to put the WEC system into the best mode of wave power capture. The critical mass of the submerged body M_c is defined by the stable boundary of the PTO spring (namely, if $M_s < M_c \rightarrow k_{pto} < 0$ and if $M_s \ge M_c \rightarrow k_{pto} \ge 0$), as illustrated in Fig. 3(a). One should notice that always $M_c < M_o$.

Each design requires a series of simplifications and assumptions to start the process. Hence, in Step 1, the model's body is imagined to be positioned sufficiently far from the water surface. This assumption is typically used when analysing various two-body WECs, as demonstrated by Beatty et al. (2019), Liang and Zuo (2017), and Yi-Hsiang and Ye (2013). Consequently, the hydrodynamic coupling coefficients of the added mass and damping ($A_{bs}, A_{sb}, d_{bs}, d_{sb}$), as well as the body radiation damping d_s, can be ignored. Therefore, in this modelling step, the body is characterized solely by its total mass and linearized damping (i.e., M_s, d_{viss}).

In the next step, after designing and specifying the geometry of the submerged body, the aforementioned assumptions are removed, and all the hydrodynamic coefficients are considered in the equations of motion for calculating the model dynamics, as presented in Step 2 of Fig. 1. Considering the assumptions of Step 1 into the parameters of Eq. (11), the optimal stiffness of the PTO spring ($k_{\text{pto OPTIMAL}}$) will be obtained as:

$$k_{\text{pto OPTIMAL}} = \omega \frac{\Upsilon\Gamma + \mathrm{T}\Psi}{\mathrm{T}^2 + \Upsilon^2} = \frac{\vartheta M_s^2 + \Re M_s + \varsigma}{\lambda M_s^2 + \varpi M_s + \mu}, M_s = A_s + m_s \tag{12}$$

where the parameters are defined as:

$$\begin{gathered} \vartheta = \omega^6 d_b, \Re = 2\omega^4 (d_b + d_{viss})(\omega^2 M_b - k_{hys}), M_b = A_b + m_b \\ \varsigma = \omega^4 d_{vis_s} \{ M_b (\omega^2 M_b - 2k_{hys}) - (d_b^2 + d_b d_{vis_s}) \} + \omega^2 k_{hys}^2 d_{vis_s}, \lambda = \omega^5 \\ \varpi = \omega^3 (2 M_b \omega^2 - k_{hys}), \mu = \omega^3 (d_b^2 + 2 d_b d_{vis_s} + d_{vis_s}{}^2 - M_b k_{hys}) + \omega^5 M_b^2 \end{gathered} \tag{13}$$

In a given wave, all parameters of equation (12) are known except the body's total mass M_s, which is unknown. Considering the different values for the submerged body's total mass, the optimal stiffness for the PTO spring $k_{\text{pto OPTIMAL}}$ will be negative in one range of the total mass and

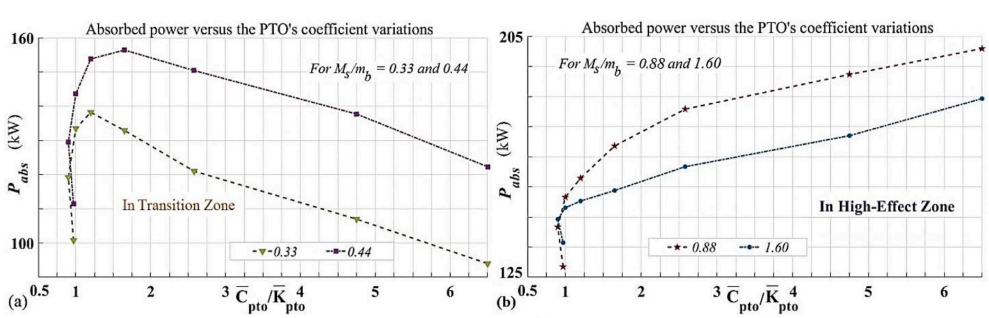

Fig. 4. Influence of the PTO's coefficients variations ($\overline{c}_{pto}/\overline{k}_{pto}$) on the absorbed power (a) in the transition zone for $M_s/m_b = 0.33$ and 0.44, (b) in the high-effect zone for $M_s/m_b = 0.88$ and 1.6.

positive in another one, as shown in Fig. 3(a) for the wave of frequency 1.1 rad/s. The turning point of this change (from the negative phase into the positive) is called the critical mass of the body M_c, which is illustrated in Fig. 3(a).

In other words, whenever the optimal stiffness of the spring in Eq. (12) is considered zero, the positive response of the equation $\vartheta {M_s}^2 + \Re M_s + \varsigma = 0$ represents the value of the critical mass M_c at each wave with frequency ω.

$$\text{If}: k_{\text{PTO}_{\text{Optimal}}} = 0 \xrightarrow{\text{Eq.12}} \vartheta M_s^2 + \Re M_s + \varsigma = 0 \xrightarrow{\text{Response } (+)} M_s = M_c \quad (14)$$

Fig. 3(a) illustrates how variations in the submerged body mass affect the optimal design of the PTO spring. For the mass values 2 times greater than the buoy's mass ($M_s/m_b > 2$), the impact of the mass variations on the optimal design is diminished, and the viscous damping term of the body ζ_s will also be ineffective.

Fig. 3(b) clearly shows the importance of optimizing the body's mass on the absorbed power and the model's efficiency. In each wave, the model's efficiency is significantly affected by changes in the body's mass and PTO's specifications, as shown in the curves of Fig. 3(b). This results also reveals the regions of the high and low-effect of the PTO's coefficient variations on absorbed power, as well as presenting a transition and irregular zone of the effect of the PTO's specification on the model's efficiency, as depicted in Fig. 3(b).

The parameters $\bar{c}_{\text{pto}}$ and $\bar{k}_{\text{pto}}$ are the average of the optimal coefficients of the PTO system in each wave period. The values of the body's mass ratio in the transition zone are $M_s/m_b = 0.05 - 0.55$, and for the high, and low-effect regions are $M_s/m_b = 0.6 - 2.1$, and 2.1 and more, respectively, as shown in Fig. 4. In low-effect zone, there is no significant effect on the absorbed power due to the body's mass changes or PTO's specification variations.

At any given value of the body's mass, the effect of the ratio $\bar{c}_{\text{pto}}/\bar{k}_{\text{pto}}$ on the absorbed power can be examined in Fig. 3(b). On the other hand, two values of the body's mass in the transition and high-effect zones are chosen to investigate the influence of the PTO's coefficients variations on the absorbed power, as illustrated in Fig. 4.

In the transition zone, as the curves in Fig. 4(a) for the values of 0.33 and 0.44 of the body's mass ratio suggest, by increasing the ratio $\bar{c}_{\text{pto}}/\bar{k}_{\text{pto}}$, the absorbed power initially rises and then immediately decreases. In this range of the body's mass values, there is no uniform effect of the ratio $\bar{c}_{\text{pto}}/\bar{k}_{\text{pto}}$ on the absorbed power, first rapidly ascending then moderate descending. While in the high-effect zone, the absorbed power always increases with increasing the PTO's coefficients ratio, as can be seen in Fig. 4(b). All in all, the curves in Fig. 3(b) to Fig. 4(b) indicate the importance of mass optimisation on the model's efficiency and the PTO's optimal coefficients.

To calculate the optimum mass of the body M_o, one can use the derivative of the absorbed power equation (Eq. (9)) with respect the total mass M_s under the PTO optimal conditions (namely, $k_{\text{pto}} = k_{\text{pto OPTIMAL}}$ and $c_{\text{pto}} = c_{\text{pto OPTIMAL}}$). Hence, substituting Eq. (11) into Eq. (9), the absorbed power will be computed as:

$$\begin{cases} \text{If}: \dfrac{d(P_{\text{abs Optimal}})}{dM_s} = 0 \ (k_{\text{pto}} = k_{\text{pto}_{\text{OPTMAL}}} \ \& \ c_{\text{pto}} = c_{\text{pto OPTMAL}}) \Rightarrow M_s = M_o \\ P_{\text{abs Optimal}} = 0.5\omega^2 \left| \dfrac{(\Pi + i\Theta)\left(\frac{\Psi^2 + \Gamma^2}{T^2 + \Upsilon^2}\right)^{\frac{1}{4}}}{\Gamma + i\Psi + (iT - \Upsilon)\left(\frac{\Psi^2 + \Gamma^2}{T^2 + \Upsilon^2}\right)^{\frac{1}{2}} + \frac{\Upsilon\Gamma + T\Psi}{T^2 + \Upsilon^2}(T + i\Upsilon)} \right|^2 \\ (\Pi, \Theta, \Psi, \Gamma, T, \Upsilon, \ldots) = f\propto(\omega, m_b, d_b, A_b, k_{\text{hys}}, M_s, d_{\text{vis}_s}, A_s, A_{bs}, \ldots.) \end{cases} \quad (15)$$

All parameters of the above equation are given except the body's total mass M_s. If the derivative of the above equation equals zero, $d(P_{\text{abs Optimal}})/d(M_s) = 0$, the response will be the optimum mass of the body M_o. The influence of the body mass changes on the absorbed power is investigated in the PTO's optimal mode. The findings are presented in Fig. 5. Specifically, Fig. 5(a) displays the position of the critical mass M_c and the optimum mass M_o for the body in the absorption bandwidth, while Fig. 5(b) presents the data for an incident wave frequency of $\omega = 1.1\,\text{rad/s} = \omega_{n_b}$.

The variations in the body's mass can increase the output power of the WEC model from approximately 60 kW to 160 kW, which represents an increase of about 166% in a specific wave, as illustrated in the curves of Fig. 5(b). This issue shows the importance of the submerged body's mass and the calculation of its optimal mass.

Fig. 5(a) shows that the mass variations of the body in the range of the buoy's natural frequency ($\omega_{n_b} = 1.1$ rad/s) have a disturbing behaviour both at the optimum and critical masses. In the absorption bandwidth, the maximum critical mass M_c is 0.64 m_b that occurs at the frequency of 1.075 rad/s and $\zeta_s = 0.15$. The minimum optimum mass M_o is 0.66 m_b observed at the frequency of 1.1 rad/s and $\zeta_s = 0.1$.

Based on the three reasons, the submerged body mass is considered

Table 1
Values of $P_{\text{abs Optimal}}$ in the range of optimum mass M_o under $\omega = 1, 1.1, 1.2$ rad/s

Within the optimum mass range of the submerged body M_o		Wave frequency ω, Wave amplitude: 1m	
$\Delta P_{\text{abs Optimal}}$ (kW)	$P_{\text{abs Optimal}}$ (kW)	The body's viscous damping coefficient ζ_s	
0.000	202.129	$\zeta_s = 0.100$	$\omega = 1.00$ rad/s
0.669	201.460	$\zeta_s = 0.125$	
0.080	201.540	$\zeta_s = 0.150$	
0.000	160.428	$\zeta_s = 0.100$	$\omega = 1.10\ \text{rad/s} = \omega_{n_b}$
0.078	160.506	$\zeta_s = 0.125$	
0.239	160.745	$\zeta_s = 0.150$	
0.000	129.699	$\zeta_s = 0.100$	$\omega = 1.20$ rad/s
0.022	129.721	$\zeta_s = 0.125$	
0.017	129.704	$\zeta_s = 0.150$	

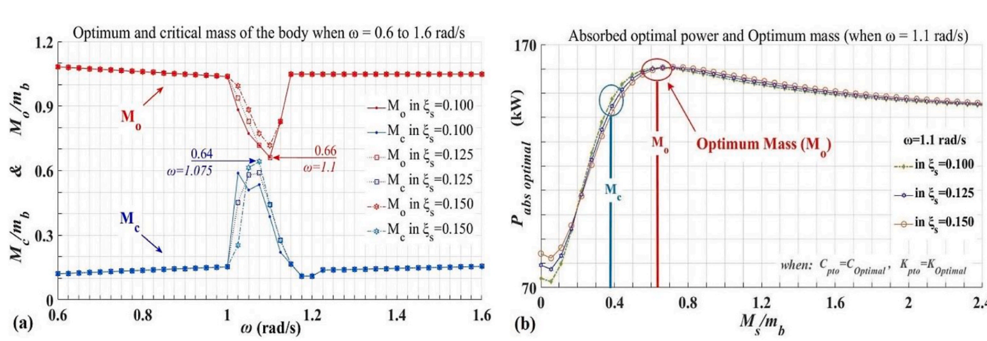

Fig. 5. (a) Optimum and critical mass of the body under the waves of absorption bandwidth $\omega = 0.6 - 1.6$ rad/s, (b) Effect of the mass variations of the body on absorbed power under the wave $\omega = 1.10\ \text{rad/s} = \omega_{n_b}$ and in $\zeta_s = 0.1, 0.125, 0.15$

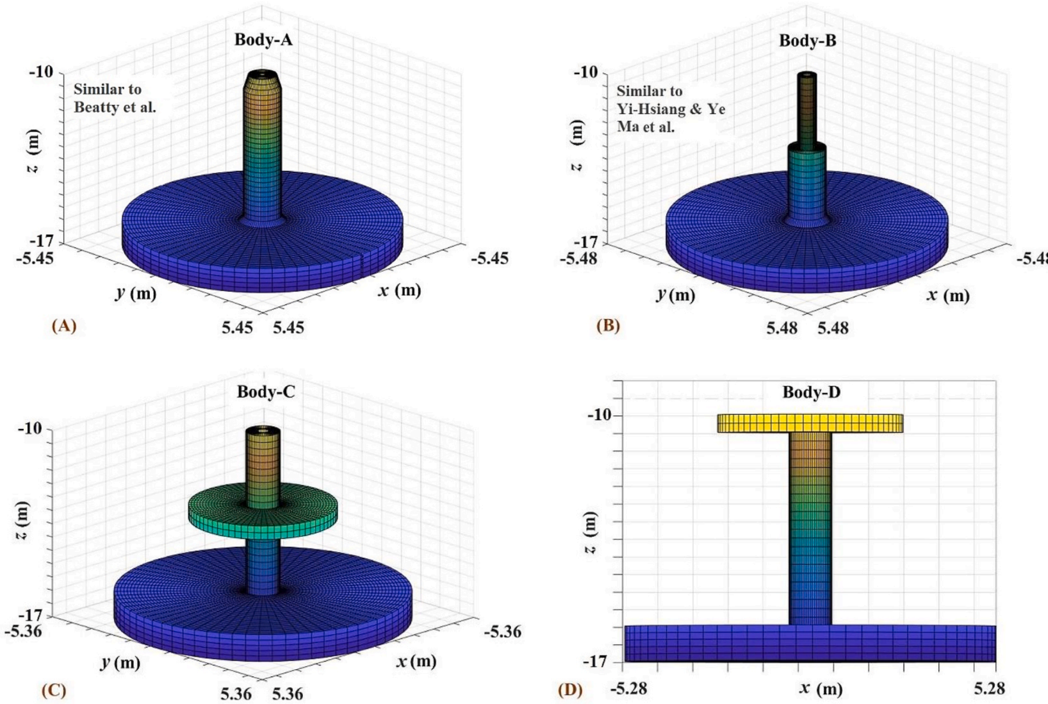

Fig. 6. Different geometries for the submerged body (the model's body) with the same total mass.

to be $0.66m_b$, which is the lowest value of the optimum mass M_o within the buoy's absorption bandwidth (see Fig. 5-a). First, the maximum captured energy occurred in the heaving resonance of the buoy when the incident wave frequency matches the natural frequency of the absorber buoy in heave motion (namely, $\omega = \omega_{n_b} = 1.1$ rad/s). Therefore, based on the curves of Fig. 5(b) that show the effect of the submerged body's mass variations on the absorbed power in the wave of frequency 1.1 rad/s, the best mass for the body is $0.66m_b$, as the other values reduce the absorbed power. Second, the submerged body is designed to enhance the buoy's efficiency (the buoy's best performance occurred for submerged body masses close to those illustrated in Fig. 5-b). Third, increasing the submerged body mass beyond the optimum mass ($M_o = 0.66m_b$) both raises the cost of the submerged body structure and reduces its efficiency, as evident in Fig. 5(b).

The intriguing aspect of the results is the low importance of the submerged body's viscous damping ζ_s on the absorbed power, exclusively within the range of the optimum mass and under Step 1 conditions, as suggested in Fig. 5 and Table 1. Additionally, findings by Liang and Zuo (2017) showed that the growth or reduction of the body's viscous damping graph ζ_s has a negligible influence on the absorbed power in the range of the body's optimum mass.

It is worth noting that the calculation is performed according to the conditions specified in Eq. (16). In other situations, the results will, however, differ. The marine environment and two-body WEC system have many variables and unpredictable conditions. Hence, simplifications and assumptions are both necessary and reasonable. It is noteworthy that the viscous effects on the body are considered in the second step of the design process.

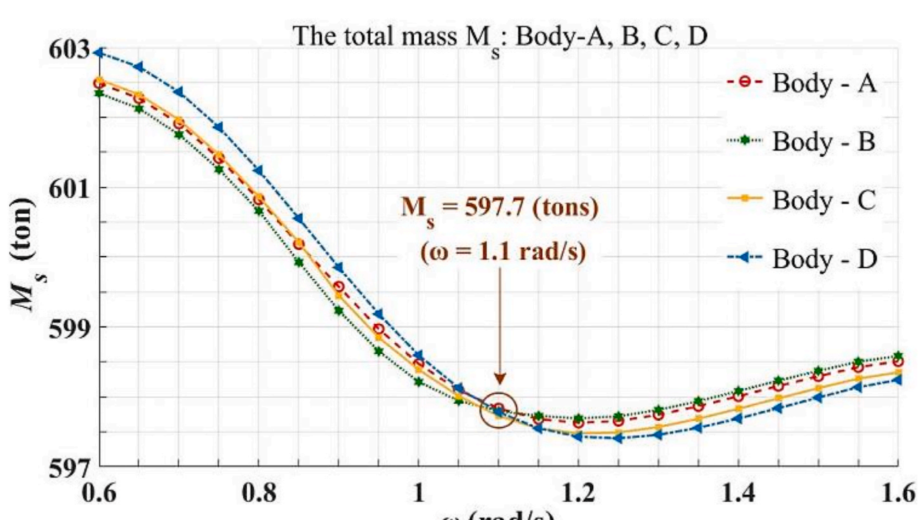

Fig. 7. Total mass of the proposed bodies A, B, C, and D under the waves of the absorption bandwidth.

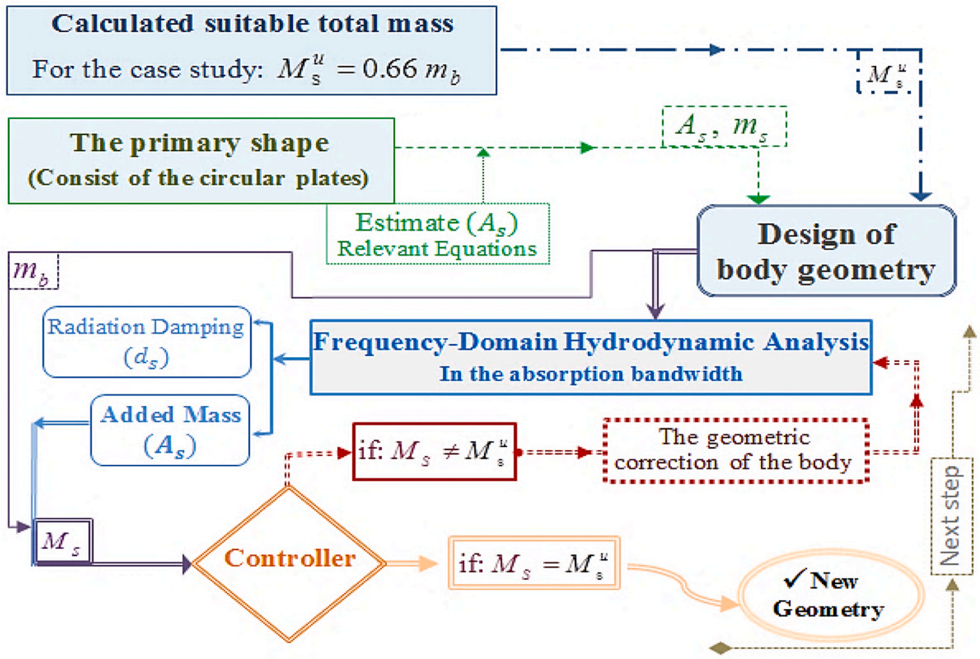

Fig. 8. Schematic diagram of the geometric selection procedure for the body with the same total mass.

$$\text{The buoy and its absorption bandwidth are given}\left\{\begin{array}{l}\text{The } k_{\text{pto}} \text{ is always positive } (+)\\ k_{\text{pto}} = k_{\text{pto}_{\text{Optimal}}},\ c_{\text{pto}} = c_{\text{pto}_{\text{Optimal}}}\\ \zeta_s = 0.1, 0.125, 0.15\\ \text{Always } M_c < M_s \le M_o\\ \text{If}: k_{\text{pto}_{\text{Optimal}}} = 0 \xrightarrow{\text{Eqs.12--14}} M_s = M_c\\ \text{If}: dP_{\text{abs}_{\text{Optimal}}} \Big/ dM_s = 0 \xrightarrow{\text{Eq.15}} M_s = M_o\end{array}\right\} \xrightarrow{\quad} \text{Step 1 Result of } M_s = 0.66\, m_b \tag{16}$$

2.5.1. Submerged body shape

As expressed in the introduction, the heave plate is a vital component of the body geometry and should be considered in its computation process. The heave plate is commonly used in the design of submerged bodies for various WEC devices, as suggested by Beatty et al. (2019), Yi-Hsiang and Ye (2013), and Ma et al. (2020). Moreover, any geometry designed for the submerged body (the model's body) must be symmetrical and have an identical total mass, which in the previous subsection was obtained as 0.66 m_b for this case study. The geometries developed for the model's body (submerged body), all maintaining the same total mass, are shown in Fig. 6.

Equalising the total mass across bodies with different shapes creates identical conditions for comparing hydrodynamic performance and investigating the influence of body shape on the model's efficiency. In other words, when the absorber buoy geometry, the PTO's specifications, and the body's total mass are optimised for the waves of the absorption bandwidth and fixed, it is possible to study the effects of the body shape variations on the efficiency of the model in various wave conditions.

Fig. 7 shows the total mass of the proposed bodies under wave excitation at different frequencies $\omega = 0.6 - 1.6$ rad/s. In the wave with frequency 1.1 rad/s, the buoy's natural frequency, the total mass for all bodies is the same ($M_s \cong 597.75$ tons $\cong M_o = 0.66\, m_b$) as marked in Fig. 7 by a circle. In other frequencies, the total mass of the studied bodies (A, B, C, and D) is not the same, but is within an acceptable range.

The geometric design of the model's body (submerged body) is carried out according to the methodology illustrated in Fig. 8, as described in the previous subsections. In the beginning, simple geometry with at least one circular plate (the heave plate) is considered for the model's body so that its total mass is approximately equal to the calculated suitable total mass ($M_s^u = 0.66\, m_b$). The added mass of the model's body is initially calculated using equations for bodies vibrating translationally in one direction in an infinite and still fluid (e.g., $A_s = 8\rho r_s^3/3$ for the heaving-submerged circular plate, as suggested by Kaneko et al. (2014). Therefore, the heave plate's diameter of all designed bodies is considered to be the same or close to each other, as seen in Fig. 6. Then, a frequency-domain analysis is performed using the Boundary Element Method (BEM) to compute the body's hydrodynamic added mass in waves. Subsequently, the body's total mass should be verified within a single controller box, as depicted in Fig. 8. This process continues until the desired body shape is created based on the defined design principles.

3. Model analysis

To perform a frequency-domain analysis utilizing the BEM, the body's hydrodynamic coefficients are calculated. This boundary method is effective for solving problems involving the interaction of the incident wave with the submerged body (referred to as the body). A right-handed coordinate system (*o-xyz*) is used, the o-*z* axis points upward against gravity, while the o-*xy* plane is parallel to the water free surface.

In the assumed computational domain, the fluid flow is assumed to be ideal and irrotational, so Laplace's equation governs the entire domain. Considering the regular waves with insignificant surface tension, the total potential ϕ arising from the interaction between the wave and the body can be described as comprising three wave components: the incident wave potential ϕ_0, the scattering potential ϕ_7, and the radiation velocity potential ϕ_j (Wang et al., 2011; Yi-Hsiang and Ye, 2013).

$$\phi(x,y,z,t) = \mathrm{Re}\left\{\left(\sum_{j=1}^{6} \xi_j\, \phi_j(x,y,z) + a_\omega\, \phi_A(x,y,z)\right)e^{i\omega t}\right\}, \phi_D = \phi_0 + \phi_7 \tag{17}$$

$$\nabla^2\phi = 0, \phi \in \Omega, \phi_0 = \frac{iga_\omega}{\omega} e^{\left(\nu z_s - i\nu x_s \cos\beta - iy_s\nu \sin\beta\right)}, \nu = \omega^2 \Big/ g, i = \sqrt{-1} \tag{18}$$

In this context, ξ_j ,$j = 1, \dots, 6$ represents the oscillatory complex amplitudes of the body (the submerged body) for six degrees of freedom, while β indicates the wave propagation angle relative to the positive x-axis ($\beta = 0$) (Yang, 2000; Berenjkoob and Ghiasi, 2016). The linear boundary conditions for the seabed and the water free surface are denoted as $\partial\phi/\partial n = 0$ and $\partial^2\phi/\partial t^2 + g(\partial\phi/\partial z) = 0$, respectively. The infinity boundaries in the computational domain and the exterior surface of the body are also described as $\lim_{x\to\pm\infty}[\partial\phi/\partial x \pm i\nu \cos\beta\, \phi] = 0$ and $\partial\phi_7/\partial n = -\partial\phi_0/\partial n$ (Wang et al., 2011; Yang, 2000), respectively.

In the radiation problem, the conditions on the exterior surface of the body are $\partial\phi_{j=1,\dots,6}/\partial n = i\omega\, n_j$, for both its translational and rotational motions. Here, $n_{j=1,2,3}$ represents the Cartesian components of a unit vector on the surface of the submerged body, pointing toward the body, and also $(n_4, n_5, n_6) = (x, y, z) \times (n_1, n_2, n_3)$ (Yang, 2000).

3.1. Hydrodynamic coefficients

The integral representation of the Laplace's equation is obtained by Green's identity for the radiation and diffraction velocity potential, the equations of (19) and (20) for smooth elements are expressed as: (Yang, 2000; Berenjkoob and Ghiasi, 2016).

$$2\pi\, \phi_j(p) + \iint_{S_b} \phi_j(q) \frac{\partial G(p,q)}{\partial n_q} dS_q = \iint_{S_b} \frac{\partial \phi_j}{\partial n_q} G(p,q)\, dS_q \;\left(\text{The radiation problem}\right) \tag{19}$$

$$2\pi\, \phi_D(p) + \iint_{S_b} \phi_D(q) \frac{\partial G(p,q)}{\partial n_q} dS_q = 4\pi\, \phi_0(p) \;\left(\text{The wave diffraction problem}\right) \tag{20}$$

where $\partial/\partial n_q$ represents the normal derivative at point q of the boundary. The free-space Green's function is defined by Yang (2000) as follows:

$$G(p,q) = \frac{1}{r} + \frac{1}{r_1} + 2\nu\, \mathrm{PV} \int_0^\infty \frac{1}{\tau - \nu} e^{\tau(z_s+\zeta)} J_0(\tau R) d\tau - 2\pi i\nu e^{\tau\,(z_s+\zeta)} J_0(\nu R) \tag{21}$$

where R expresses the length between the source point and the flow field point, defined as $R^2 = (x-\xi)^2 + (y-\eta)^2$. Likewise, $r_1{}^2 = R^2 + (z+\zeta)^2$, and $r^2 = R^2 + (z-\zeta)^2$. In the radiation problem, the six components of force and moment can be expressed in matrix form as follows:

$$F_k = \mathrm{Re}\left\{\sum_{j=1}^{6} \xi_j e^{i\omega t} f_{kj}\right\}, k, j = 1, \dots, 6, f_{kj} = -\rho \iint_{S_0} \frac{\partial \phi_k}{\partial n} \phi_j ds \tag{22}$$

In the radiation problem, the index f_{kj} denotes the complex force coefficient of the body. The hydrodynamic coefficients of the body, which consist of added mass A_{kj} and radiation damping d_{kj}, can be defined as components of the force represented by f_{kj}: $f_{kj} = \omega^2 A_{kj} - i\omega\, d_{kj}$ (Yang, 2000; Ma et al., 2020). The subscripts k and j refer to the six directions of body motion.

First, a submerged body is designed according to the dimensions and shape in the work of Ma et al. (2020) to validate the results and the computational method. The body geometry is exactly like Body-B in Fig. 6. When the radiation velocity potential is obtained from Eq. (19), the added mass and damping coefficients of the model's body (the submerged body) are calculated. Fig. 9 is presented and compared the present results under different panels with Ma et al. (2020).

Fig. 9 illustrates how growing the number of elements (panels) from 2416 to 6396 affects the computation error. As the number of body-geometry panels increases, the results approach those of Ma et al. (2020), indicating that the solutions converge with greater accuracy. Nevertheless, the mere increase in elements does not significantly contribute to validating the results. In the different panels, the relative error is calculated via Eq. (23) and then compared with the findings of Ma et al. (2020) as shown in Fig. 10.

$$\text{Relative error} = \gamma_{(\%)} = \left|\frac{\text{Results}_{\text{Ma et al.}} - \text{Results}_{\text{Present}}}{\text{Results}_{\text{Ma et al.}}}\right| \times 100 \tag{23}$$

Within the absorption bandwidth, the hydrodynamic coefficients of the proposed bodies are computed using the BEM by solving their radiation problem. The added mass and radiation damping of the bodies, as well as their coupling coefficients resulting from the motion interactions between the absorber buoy and each of the submerged bodies (A, B, C, and D), are illustrated in Figs. 11–13.

In the second modelling step, all hydrodynamic coefficients are crucial parameters in calculating the model's dynamics under wave

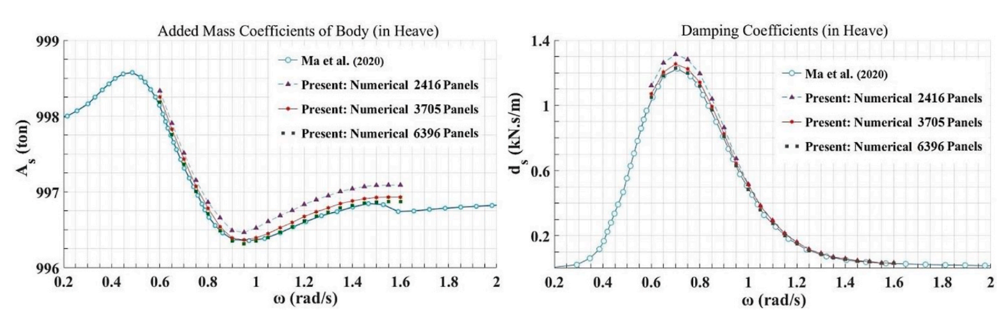

Fig. 9. Comparison between the radiation damping d_s and added mass A_s results from the current study with those of Ma et al. (2020).

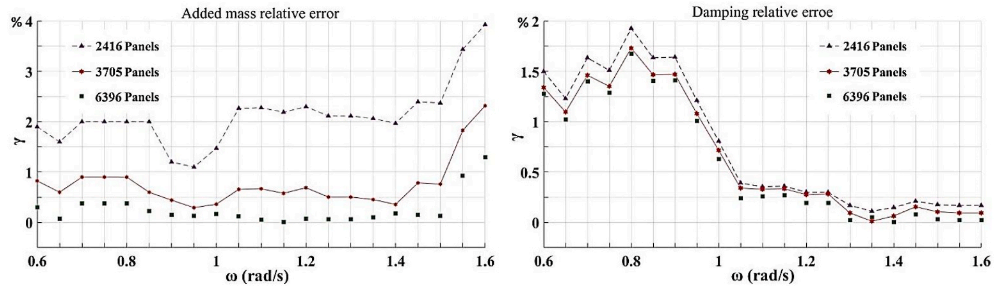

Fig. 10. Relative error associated with the hydrodynamic added mass and damping, for 2416 to 6396 panels.

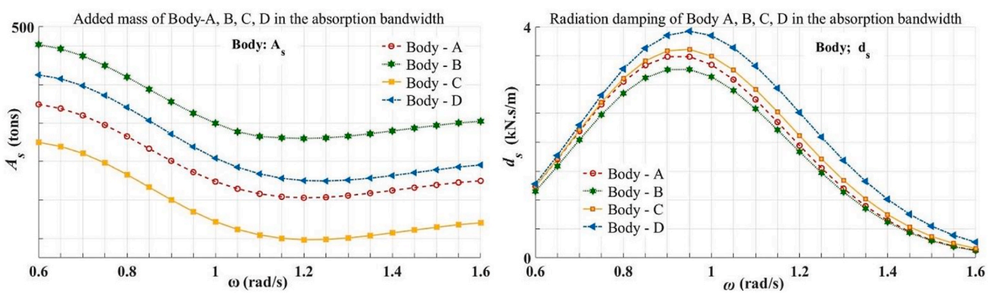

Fig. 11. Added mass A_s and damping d_s for the proposed bodies within the absorption bandwidth.

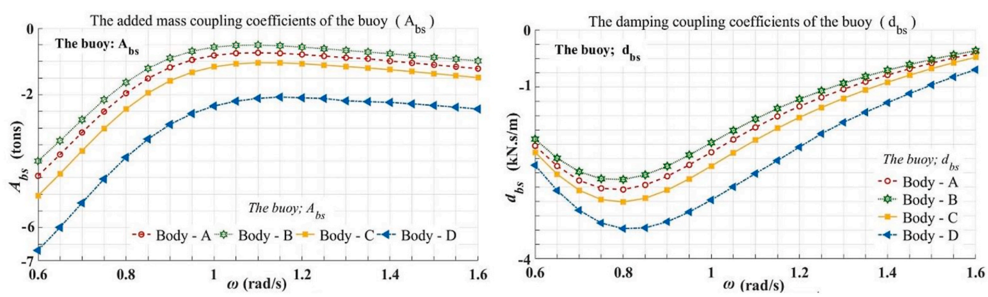

Fig. 12. Hydrodynamic coupling coefficients of the absorber buoy caused by the presence of any submerged body A to D.

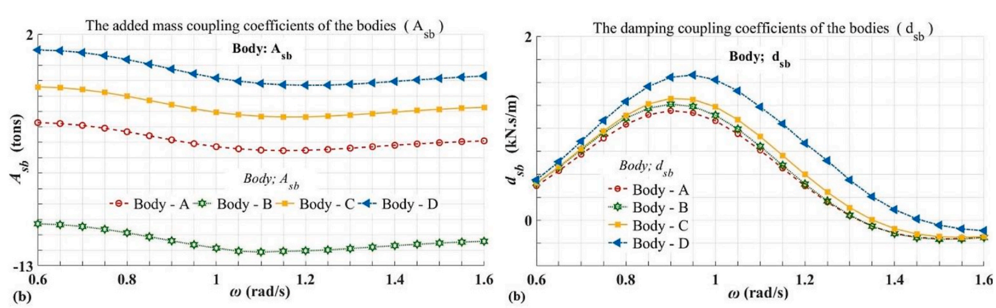

Fig. 13. Hydrodynamic coupling coefficients of submerged bodies A to D; their added mass and damping A_{sb}, d_{sb}.

excitations, as described in Eqs. (1)–(8) and seen in step 2 of Fig. 1. These coefficients depend on the wave characteristics and the geometry of the model's buoy and body. Note that for a given wave and while the buoy geometry remains fixed in the WEC model, any geometric changes of the model's body affect the coupling coefficients of the absorber buoy (A_{bs}, d_{bs}) as illustrated in Fig. 12.

The hydrodynamic coupling coefficients reflect the influence of the body's hydrodynamics on the absorber buoy's hydrodynamic coefficients, and vice versa. Here, the coupling coefficients of the absorber buoy indicate a difference in two modes: the presence and absence of the body. For example, the coupling coefficient of the buoy's added mass, referred to as A_{bs}, is calculated by finding the difference between the buoy's added mass in the absence of the body (denoted as A_b) and in the presence of the body (denoted as A_b'): namely, $A_{bs} = A_b - \mathrm{A}_\mathrm{b}'$ and also, $d_{bs} = d_b - \mathrm{d}_\mathrm{b}'$). In other words, parameters A_b and d_b are the absorber buoy's added mass and its radiation damping during its free oscillation, which occurs in the absence of the submerged body, respectively.

Fig. 12 shows that the buoy's coupling coefficients are negative (namely, $\mathrm{A}_\mathrm{b}' > A_b$ and $\mathrm{d}_\mathrm{b}' > d_b$). It also suggests an additive effect in the buoy's added mass and its radiation damping due to the presence of the submerged body. According to the results, Body-D exhibits the highest

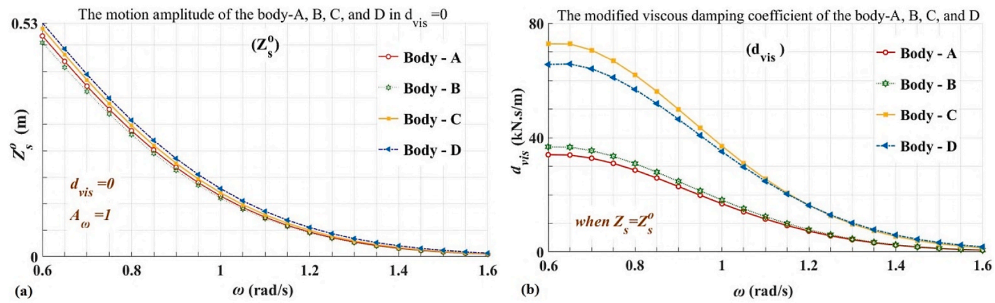

Fig. 14. Heave amplitude under the condition of no viscosity Z_s^0 and the modified viscous damping d_{vis_s} for the submerged bodies A to D.

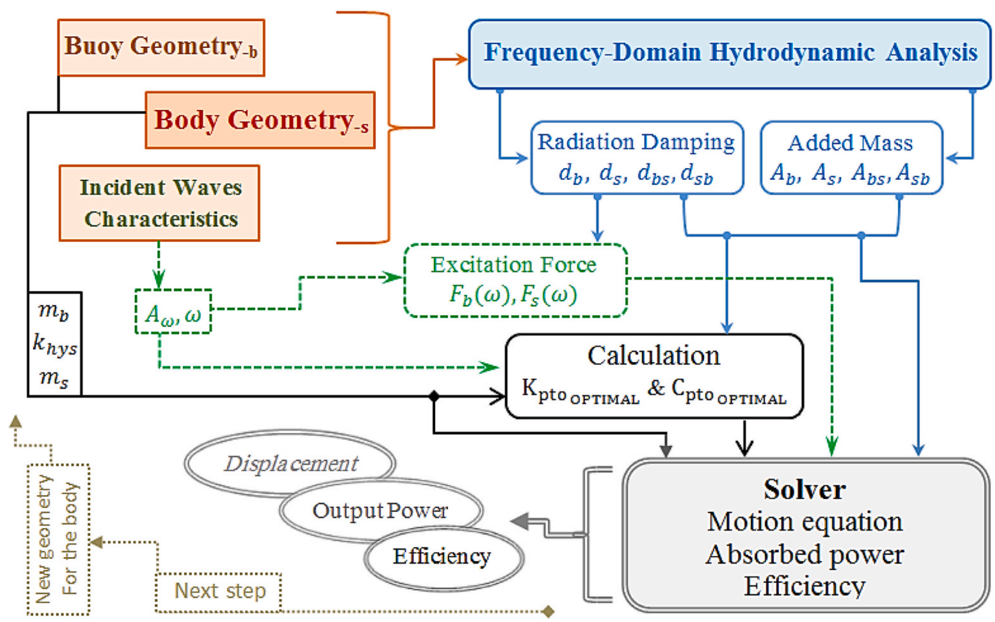

Fig. 15. Flowchart for the computational analysis of the two-body WEC dynamic model until its output power and efficiency (Step 2 in Fig. 1).

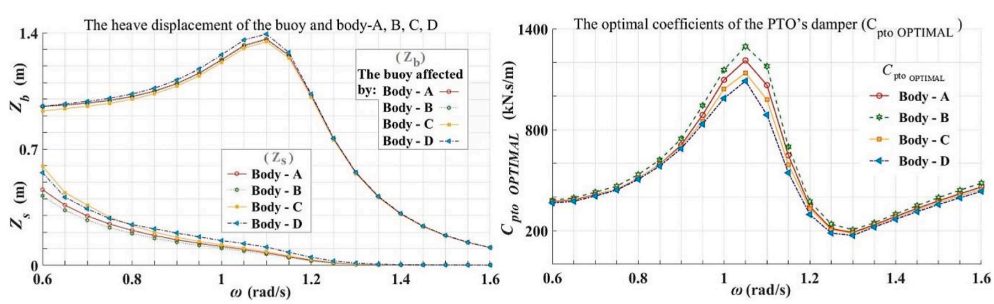

Fig. 16. PTO's optimal damping $C_{\mathrm{pto\ OPTIMAL}}$ and the buoy's and body's heave displacement.

increase in the hydrodynamic coefficients of the absorber buoy (see Fig. 12). Therefore, submerged Body-D will have the worst effect on the buoy's performance.

After calculating all hydrodynamic coefficients ($A_b, A_s, d_b, d_s, A_{bs}, A_{sb}, d_{bs}, d_{sb}$), one can proceed to the second modelling step, as shown in Fig. 1. In this step, the WEC model is separately equipped with Bodies A, B, C, and D, while the model's absorber buoy remains unchanged as its main component.

For Step 2, all the hydrodynamic parameters in the equation of the motion and absorbed power are specified and calculated by the well-known BEM (Eqs. (1)–(8) and (15)). However, the viscous term of the body d_{vis_s} is calculated by an approximate equation (Eq. (3)) proposed by Liang and Zuo (2017). This equation is a suitable approximation only for the first step of modelling (Step 1), which involves calculating a suitable total mass for the model's body and then the geometric design of the model's body. The body's physical parameters are not included in this equation because, at step 1, the model's body is considered to have no geometry. Therefore, in Step 2, the viscous damping of the bodies should be calculated based on their geometry and hydrodynamics.

3.2. Additional viscous damping of the body

The dynamics of the body are affected by fluid viscosity, especially during heave motion. The viscous term is influenced by flow separation

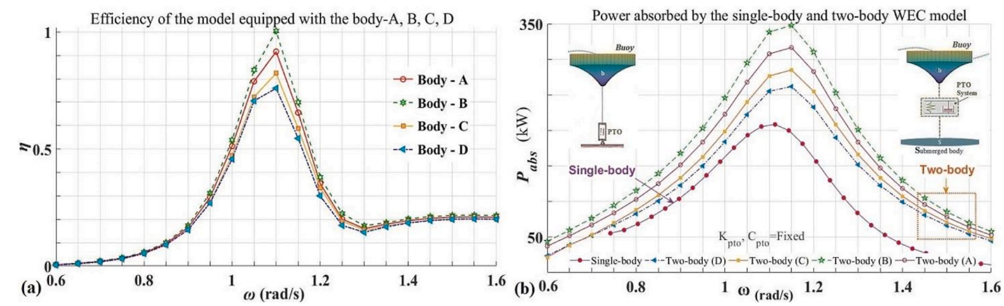

Fig. 17. (a) Efficiency of the model equipped with different submerged bodies (η), (b) the power absorbed by the single-body system of Berenjkoob et al. (2021) and the two-body WEC model.

and vortices, as well as by friction due to fluid shear stress on the body. Hence, to account for the influences of viscous terms, a drag force is included in the motion equation of the model's body, which is proportional to the body's dimensions and its dynamics in the wave ($F_{\text{drag}} = 0.5\rho S_s C_d \dot{z}_s|\dot{z}_s|$). Using Lorentz linearization, the force is replaced by a linear damping term expressed as $f_{\text{drag}} = (4i/3\pi)\rho\omega^2 S_s C_d |Z_s| Z_s = d_{\text{vis}_s} Z_s$, as described by Xu et al. (2019b), where S_s represents the cross-sectional area of the model's body in heave, which is equivalent to $S_s = \pi D_s{}^2/4$ for the heave plate shape. The drag coefficient, C_d, is affected by the body geometry, Reynolds number, and the Keulegan–Carpenter number ($K_C = 2\pi a_s/D_s$). Here, a_s signifies the motion amplitude of the body and D_s denotes its characteristic diameter.

The linearized viscous drag coefficient is assumed to be $C_d = \delta_s K_C{}^{-1/3} = \delta_s(2\pi a/D_s)^{-1/3}$, as stated by Xu et al. (2019b). Here, the value of δ_s is dependent on the body's geometry and determined as 3.5 for the geometry of Body-B based on the experimental results of Xu et al. (2019b) (i.e., $\delta_s = 3.5$). Therefore, the viscous damping term of the body in Eq. (3) is modified as follows:

$$d_{\text{vis}_s} = 0.18\, i\delta_s\rho\omega^2\left(\frac{D_s^7}{Z_s}\right)^{1/3}|Z_s| \text{ In Step 2} \tag{24}$$

The modified viscous coefficient for the body is incorporated into the equations of motion and absorbed power (Eqs. (7), (8) and (16), respectively) and calculated during each computational iteration. Initially, the motion amplitude of the body is calculated under the condition of no viscous damping. Using this newly calculated amplitude (denoted as Z_s^0), the coefficient d_{vis_s} is derived as shown in Fig. 14. The impact of the body's dimensions on the viscous coefficient is demonstrated in Fig. 14(b).

4. Dynamic responses

The steady-state responses of the absorber buoy and submerged body are numerically calculated, as depicted in the flowchart of Fig. 15. In step 2, the computational process of the WEC dynamic model in the flowchart illustrates how the model operates to determine its output power and efficiency.

For each wave frequency ω, the specifications of the PTO, including stiffness and damping, are designed at the optimal mode ($k_{\text{pto OPTIMAL}}$; $c_{\text{pto OPTIMAL}}$) via Eq. (11) based on the buoy's and body's hydrodynamic and physical characteristics. The optimal values for the PTO damper are shown in Fig. 16. This design approach for the PTO system was referred to as the dynamic design or optimal variable design (Berenjkoob et al., 2021).

In heave motion, the displacement of the absorber buoy Z_b and submerged body Z_s in a coupling system is calculated through Eq. (7) as presented in Fig. 16. The results show the proximity of the oscillation amplitude of the evaluated bodies. The main reason for this proximity may be the equal mass of the proposed bodies. The mass value ($M_s = m_s + A_s = 0.66 m_b$) is computed and optimised for this range of the incident waves. The effect of the total mass is dominant over other parameters affecting the submerged body's heave motion.

The model's output power is obtained in the PTO's optimal mode using Eq. (15) within a heaving coupling system. The model's efficiency, η, is calculated by dividing the absorbed power by the highest power that an axisymmetric buoy can theoretically extract from regular waves in heave (Khojasteh and Kamali, 2016).

$$\eta = \frac{P_{\text{abs Optimal}}}{P_{\max}}, P_{\max} = \frac{\rho g^2 A_\omega^2}{4\omega} C_w \tag{25}$$

The maximum capture width of the wave energy for the axisymmetric buoy is specified by $C_w = g/\omega^2$ in deep-water waves (Khojasteh and Kamali, 2016). According to the results, Body B had the best version in the wave-power extraction process, while submerged bodies A, C, and D ranked second, third, and fourth, respectively (as shown in Fig. 17-a).

The model's performance is compared with that of a single-body model proposed by Berenjkoob et al. (2021) to show the impact of using a submerged body on energy absorption efficiency. The results show a rate of increase 20 to 62 percent on the absorbed power when converting from the single-body WEC system into the two-body WEC model.

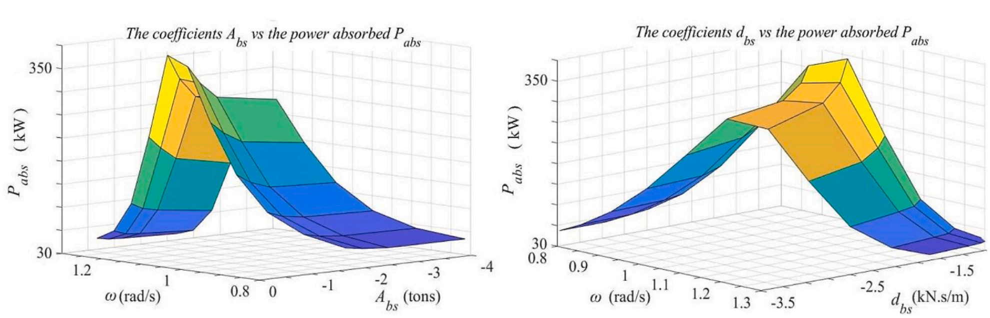

Fig. 18. Influence of coupling coefficients A_{bs} and d_{bs} on absorbed power P_{abs}.

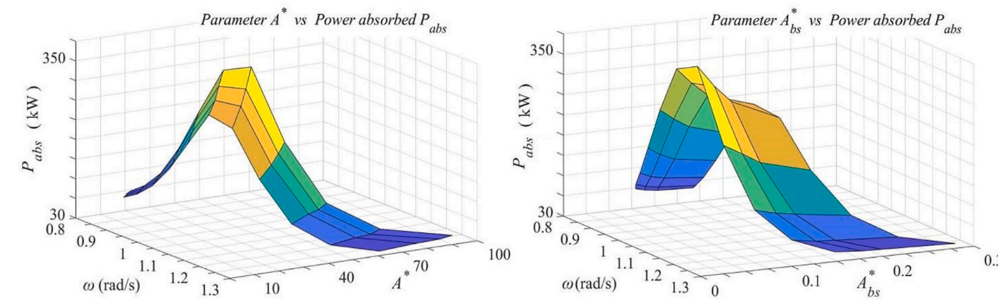

Fig. 19. Influence of parameters A^* and A^*_{bs} on absorbed power P_{abs}.

For the two-body WEC model optimised in mass and shape, the maximum power is absorbed about 344 kW, which is about 62% more power than the single-body WEC system (212 kW) in the resonance region of the model's absorber buoy, as depicted in Fig. 17(b).

Comparing the curves in Figs. 17 and 5(b) clearly indicates that variations in the body's mass can significantly increase energy absorption efficiency compared to changes in the body's shape, underscoring the importance of the submerged body's mass over its geometric shape.

5. Parametric sensitivity analysis

The hydrostatic and hydrodynamic terms of the absorber buoy and submerged body of the WEC model, along with the PTO's specifications, are among the effective parameters that significantly affect the model's dynamics and efficiency. In Fig. 1, the model's buoy is predefined, while its submerged body is designed to have a specified total mass ($M_s^u = 0.66m_b$, which was calculated in Step 1). Moreover, the optimal stiffness and damping of the PTO system are calculated based on the hydrodynamic parameters of both the proposed body and the pre-specified buoy. Hence, it is possible to explore the effect of the body shape on the energy-absorption performance of the WEC model solely, since the buoy remains unchanged from the outset of the modelling.

The results indicate that if the body geometry can reduce the added mass and radiation damping of the absorber buoy compared to its free oscillation (i.e., $\mathrm{A}_\mathrm{b}' < A_b$ or $A_{bs} > 0$), it will increase the absorption efficiency. In other words, in the process of comparing the various geometries of the submerged body with similar total mass, the geometry capable of reducing the parameters A_b' and d_b' (i.e., enhancing the hydrodynamic coupling coefficients of the absorber buoy) will be more desirable (reminder, $A_{bs} = A_b - \mathrm{A}_\mathrm{b}'$ and $d_{bs} = d_b - \mathrm{d}_\mathrm{b}'$). As the curves in Fig. 18 suggest, by increasing the parameters A_{bs} or d_{bs} by altering the body geometry, the power absorbed rises in any wave with a frequency of ω. The peak power is absorbed in the buoy's natural frequency ($\omega = 1.1\ \mathrm{rad/s} = \omega_{n_b}$).

To simultaneously investigate the effects of the added mass and radiation damping, two dimensionless parameters are presented: $A^* = A_s/(d_s \times T_\omega)$ and $A^*_{bs} = A_{bs}/(d_{bs} \times T_\omega)$. The wave period is defined in this context by an index T_ω. Fig. 19 illustrates the direct effect of the parameter A^*, which is the ratio of the body's added mass to its radiation damping, on power absorption. The results show that the submerged body with the higher A^* value yields greater power absorption by the WEC model, and vice versa, regardless of the incident wave frequency. In other words, a rise in the dimensionless parameter A^* will lead to higher absorbed power in any wave. This trend, however, reverses for the parameter A^*_{bs}.

To enhance absorption efficiency in the WEC model, the body geometry must reduce the parameter A^*_{bs}, as seen in Fig. 19. Therefore, these two criteria can be employed to compare the various geometries of the submerged body to select an appropriate one. This comparison is conducted while maintaining a constant total mass for each proposed body and treating the buoy as the unchangeable, fixed, main component of the WEC model.

6. Conclusions

In this paper, a procedure is presented for designing the submerged body to minimise the total mass of a two-body WEC system. To this end, three modelling steps are considered: conceptual modelling, modelling to determine the optimal total mass, and modelling to analyse the dynamics of the two-body WEC model, using two default values for the buoy geometry and the wave characteristics. The viscous damping for the body is considered and incorporated into the equations of motion and absorbed power during the second design step.

The total mass of the body is calculated based on the motion equations of the two-body WEC system, the optimal mode equations of the PTO system, the derivatives of the absorbed power equation, and the hydrodynamic specifications of a pre-specified buoy and its wave-energy absorption bandwidth. The critical and optimum mass values (labelled as M_{c} and, respectively) determine the optimal mass of the model's body while the PTO system is operating in its optimal mode. The optimal mass calculation method effectively reduces the design steps for the submerged body (the body), serves as a criterion for selecting an improved design, and ensures the stability of the PTO system. The body's mass variations can increase output power by 166% for a specific wave, underscoring the importance of the submerged body's mass. For the defined waves, the submerged body's optimal mass is 66% of the model's buoy mass.

In terms of effectiveness in wave energy absorption, four key criteria of A^*, A^*_{bs}, A_{bs}, and d_{bs} effectively aid in comparing different bodies and identifying the best one. The findings reveal that by increasing the values of parameters A^*, A_{bs}, and d_{bs}, through modifications to the geometry of the model's body, the corresponding absorbed power is enhanced in each wave. It can be concluded that a geometric shape of the body with the capability of reducing the added mass and radiation damping of the model's buoy compared to its free oscillation (i.e., $\mathrm{A}_\mathrm{b}' < A_b$ so $A_{bs} > 0$) can significantly enhance absorption efficiency. The mass optimisation and shape adaptation for the submerged body of the two-body WEC model can generate about 20% to 64% more power than the single-body WEC.

All in all, the concept of total mass in the body design (calculated based on the specification of a predefined buoy and its absorption bandwidth at the optimal mode of the PTO system) can be regarded as an effective method for determining an initial criterion for the submerged body.

CRediT authorship contribution statement

Mahdi Nazari Berenjkoob: Formal analysis, Methodology, Validation, Visualization, Writing – original draft. **J.F.M. Gadelho:** Writing – review & editing. **Hassan Ghassemi:** Supervision, Writing – review & editing. **C. Guedes Soares:** Supervision, Writing – review & editing.

Declaration of competing interest

The authors declare that they have no known competing financial interests or personal relationships that could have appeared to influence the work reported in this paper.

Acknowledgements

This work contributes to the Strategic Research Plan of the Centre for Marine Technology and Ocean Engineering (CENTEC), which is financed by the Portuguese Foundation for Science and Technology (Fundação para a Ciência e Tecnologia - FCT) under contract UID-00134-2025 (https://doi.org/10.54499/UID/00134/2025).

References

Ahmed, A., Wang, Y., Azam, A., Zhang, Z., 2022. Design and analysis of the bulbous-bottomed oscillating resonant buoys for an optimal point absorber wave energy converter. Ocean Eng. 263, 112443. https://doi.org/10.1016/j.oceaneng.2022.112443.

Beatty, S.J., Bocking, B., Bubbar, K., Buckham, B.J., Wild, P., 2019. Experimental and numerical comparisons of self-reacting point absorber wave energy converters in irregular waves. Ocean Eng. 173, 716–731. https://doi.org/10.1016/j.oceaneng.2019.01.034.

Berenjkoob, M.N., Ghiasi, M., Guedes Soares, C., 2019a. On the improved design of the buoy geometry on a two-body wave energy converter model. J. Renew. Sustain. Energy 11, 054702. https://doi.org/10.1063/1.5095871.

Berenjkoob, M.N., Ghiasi, M., Guedes Soares, C., 2019b. Performance of two types of mooring systems in the heave motion of a two-body floating wave energy converter. J. Mar. Sci. Appl. 18, 38–47. https://doi.org/10.1007/s11804-019-00082-w.

Berenjkoob, M.N., Ghiasi, M., Guedes Soares, C., 2021. Influence of the shape of a buoy on the efficiency of its dual-motion wave energy conversion. Energy 214, 118998. https://doi.org/10.1016/j.energy.2020.118998.

Berenjkoob, M.N., Ghiasi, M., 2016. A numerical and theoretical study of wave interaction with floating vertical cylinders by boundary element method and removal of singularities in boundary integral equations. The 18th Marine Industries Conference (MIC2016), pp. 18–21. October 2016 – Kish Island.

Chen, Z., Zhang, X., 2025. Experimental investigation of the two-body wave energy converter integrated with a spring bistable mechanism and a mechanical motion rectifier. Ocean Eng. 322, 120412. https://doi.org/10.1016/j.oceaneng.2025.

Dai, S., Chai, Y., Liu, H., Yi, W., Lyu, F., Chen, H., 2025. Experimental study on power generation characteristics of a built-in bistable mechanism wave energy converter with broadband capturing performance. Ocean Eng. 339, 122126. https://doi.org/10.1016/j.oceaneng.2025.122126.

Falnes, J., Kurniawan, A., 2020. Ocean Waves and Oscillating Systems: Linear Interactions Including wave-energy Extraction, 8. Cambridge University Press.

Garcia-Teruel, A., Forehand, D., 2019. Optimal wave energy converter geometry for different modes of motion. In: Guedes Soares, C. (Ed.), Advances in Renewable Energies Offshore. Taylor & Francis, London, UK, pp. 299–305.

Gaspar, J.F., Hallak, T.S., Guedes Soares, C., Costa, M., Nepomuceno, E., 2025. Review of wave energy converter design for offshore hybrid platforms. In: Guedes Soares, C., Wang, S. (Eds.), Innovations in Renewable Energies Offshore. Taylor and Francis, London, UK, pp. 795–805. https://doi.org/10.1201/9781003558859.

Gaspar, J.F., Pinheiro, R.F., Mendes, M.J., Kamarlouei, M., Guedes Soares, C., 2024. Review on hardware-in-the-loop simulation of wave energy converters and power take-offs. Renew. Sustain. Energy Rev. 191, 114144. https://doi.org/10.1016/j.rser.2023.114144.

Giorgi, G., Ringwood, J.V., 2017. Computationally efficient nonlinear froude–krylov force calculations for heaving axisymmetric wave energy point absorbers. J. Ocean Eng. Marine Energy 3, 21–33. https://doi.org/10.1007/s40722-016-0066-2.

Hallak, T.S., Gaspar, J.F., Guedes Soares, C., 2024. A mathematical model for the dynamic analysis of multi-body floating platforms with complex mechanical constraints. Ocean Eng. 314, 119640. https://doi.org/10.1016/j.oceaneng.2024.119640.

Kaneko, S., Nakamura, T., Inada, F., Kato, M., Ishihara, K., Nishihara, T., 2014. Flow-Induced Vibrations: Classifications and Lessons from Practical Experiences. Flow-induced Vibrations, pp. 359–401. Chapter 8, Elsevier Science.

Khojasteh, D., Kamali, R., 2016. Evaluation of wave energy absorption by heaving point absorbers at various hot spots in Iran seas. Energy 109, 629–640. https://doi.org/10.1016/j.energy.2016.05.054.

Korde, U.A., 2003. Systems of reactively loaded coupled oscillating bodies in wave energy conversion. Appl. Ocean Res. 25, 79–91. https://doi.org/10.1016/S0141-1187(03)00044-0.

Li, X., Liang, C., Chen, C.A., Xiong, Q., Parker, R.G., Zuo, L., 2020. Optimum power analysis of a self-reactive wave energy point absorber with mechanically-driven power take-offs. Energy 195, 116927. https://doi.org/10.1016/j.energy.2020.116927.

Liang, C., Zuo, L., 2017. On the dynamics and design of a two-body wave energy converter. Renew. Energy 101, 265–274. https://doi.org/10.1016/j.renene.2016.08.059.

López, M., Taveira-Pinto, F., Rosa-Santos, P., 2017. Numerical modelling of the CECO wave energy converter. Renew. Energy 113, 202–210. https://doi.org/10.1016/j.renene.2017.05.066.

Ma, Yong, Zhang, A., Yang, L., Li, H., Zhai, Z., Zhou, H., 2020. Motion simulation and performance analysis of two-body floating point absorber wave energy converter. Renew. Energy 157, 353–367. https://doi.org/10.1016/j.renene.2020.05.026.

Martin, D., Wise, A., Liang, C., Zuo, L., 2017. Shape optimization for the submerged body of a two-body wave energy converter. Proceedings of the 12th European Wave and Tidal Energy Conference, EWTEC 2017, Cork, Ireland.

Pastor, J., Liu, Y., 2014. Frequency and time domain modeling and power output for a heaving point absorber wave energy converter. Int. J. Environ. Eng. 5 (2), 101. https://doi.org/10.1007/s40095-014-0101-9.

Rahimi, A., Rezaei, S., Mansourzadeh, S., Parvizian, J., 2024. Dimensional optimization of a two-body wave energy converter under irregular waves for the strait of hormuz. Ocean Eng. 292, 116539. https://doi.org/10.1016/j.oceaneng.2023.116539.

Ramos-Marin, S., Guedes Soares, C., 2025. Review of wave energy resource characterisation, metrics, and global assessments. J. Mar. Sci. Appl. 24, 53–75.

Rezanejad, K., Guedes Soares, C., 2018. Enhancing the primary efficiency of an oscillating water column wave energy converter based on a dual-mass system analogy. Renew. Energy 123, 730–747. https://doi.org/10.1016/j.renene.2018.02.084.

Wang, B., Zhou, C., Li, H., Wu, C., Zhang, J., 2025. A novel buoy optimization approach for PAWEC in sea states with seasonal wave distribution. Ocean Eng. 334, 121623. https://doi.org/10.1016/j.oceaneng.2025.121623.

Wang, K., Zhang, X., Gao, X., 2011. Study on scattering wave force of horizontal and vertical plate type breakwaters. China Ocean Eng. 25, 699–708. https://doi.org/10.1007/s13344-011-0056-z.

Xu, Q., Li, Y., Yi-Hsiang, Yu, Ding, B., Jiang, Z., Lin, Z., 2019b. Experimental and numerical investigations of a two-body floating-point absorber wave energy converter in regular waves. J. Fluid Struct. 91, 102613. https://doi.org/10.1016/j.jfluidstructs.2019.03.006.

Xu, S., Wang, S., Guedes Soares, C., 2019a. Review of mooring design for floating wave energy converters. Renew. Sustain. Energy Rev. 111, 595–621. https://doi.org/10.1016/j.rser.2019.05.027.

Yang, S.A., 2000. On the singularities of Green's formula and its normal derivative, with an application to surface-wave–body interaction problems. Int. J. Numer. Methods Eng. 47, 1841–1864. https://doi.org/10.1002/(SICI)1097-0207(20000420)47:11%3C1841::AID-NME854%3E3.0.CO;2-1864.

Yi-Hsiang, Yu, Ye, Li, 2013. Reynolds-averaged navier–stokes simulation of the heave performance of a two-body floating-point absorber wave energy system. Comput. Fluid 73, 104–114. https://doi.org/10.1016/j.compfluid.2012.10.007.

Zakaria, M.F.U.A.P., 2025. State of the art of power take off (PTO) systems in Wave Energy Converter (WEC). Ocean Eng. 335, 121669. https://doi.org/10.1016/j.oceaneng.2025.121669.